The Elemental Composition of the Corona of Procyon: Evidence for the Absence of the FIP Effect

Jeremy J. Drake,* J. Martin Laming, Kenneth G. Widing, Jürgen H. M. M. Schmitt, Bernhard Haisch, Stuart Bowyer

The chemical composition of the solar corona is not the same as that of the underlying photosphere. In the corona, elements with a first ionization potential (FIP) of ≤10 electron volts (for example, iron, magnesium, silicon, and calcium) are overabundant relative to those with an FIP of ≥10 electron volts (for example, oxygen, neon, and sulfur) by factors of 3 to 10 with respect to the photosphere. The origin of this FIP effect is unknown. The launch of the Extreme Ultraviolet Explorer Satellite (EUVE) opened up the spectroscopic capability required to determine elemental abundances in the coronae of other stars. Spectroscopic observations of the corona of the nearby F5 IV star Procyon obtained with EUVE have yielded estimates of the relative abundances of high- and low-FIP species. The results provide evidence that Procyon, unlike the sun, does not exhibit the FIP effect. Whether the sun or Procyon is more typical of the general late-type stellar population is of fundamental interest to the physics of stellar outer atmospheres and has a bearing on the origin of cosmic rays.

The suggestion that the abundances of elements in the diffuse hot (temperature $T \sim 10^5$ to 10^7 K) plasma that makes up the solar corona differ from the corresponding values in the cooler ($T \sim 6 \times 10^3$ K), more dense photosphere dates back to pioneering extreme ultraviolet (EUV) spectroscopic studies of the corona in the 1960s (*1*). Subsequent work on solar energetic particles (*2*), which originate in the solar corona, and direct x-ray and EUV spectroscopic observations of the corona (*3–5*) confirmed, upon reexamination (*6*), that the abundances of elements such as Fe, Mg, and Si are enhanced in the corona by factors of up to 10. An additional surprise was that this abundance pattern bore notable similarity to that observed in cosmic rays (*2*). A systematic underlying trend was discovered in the abundance enhancements when the elements were ordered according to their FIPs (*7*): Elements with low FIP (≤10 eV) show a clear enhancement when compared to elements with high FIP (≥10 eV), a phenomenon now commonly known as the FIP effect (*6, 8*). The highest FIP for which abundance enhancements are observed, ~10 eV, implies temperatures of ~10,000 K or so at the site of fractionation. Such temperatures occur in the solar chromosphere. However, as yet, there are no widely accepted models to explain the process responsible for the fractionation.

Do other stellar coronae share a solar-like abundance enhancement of low-FIP species, or by some rare coincidence of stellar parameters and evolutionary circumstance, are the enhancements in the solar corona unique? The only way to investigate the compositions of the coronae of other stars directly is through EUV and x-ray spectroscopy. The capability of resolving the individual spectral lines that can provide coronal abundance diagnostics at these short wavelengths has only been realized since the launch of the Extreme Ultraviolet Explorer (EUVE) satellite in 1992. The EUVE spectrometers provide moderate-resolution (wavelength $\lambda/\Delta\lambda \sim 200$) spectroscopy from 75 to 760 Å in three band passes (*9*), commonly designated short wavelength (SW), medium wavelength (MW), and long wavelength (LW). In this report, we present an analysis of the abundances of elements in the corona of a star other than the sun. Our analysis is based on EUVE spectroscopic observations of Ne and S (both high-FIP elements) and Fe, Mg, Si, and Ca (all low-FIP elements) features seen in the EUVE MW and LW spectra of the corona of the F5 IV star Procyon.

The photospheric abundances in Procyon are very well known from optical spectroscopy (*10–14*) and are, to within small experimental uncertainties (≤25%), solar. Unfortunately, although Ne lines appear prominently in coronal spectra, Ne abundances cannot be measured in late-type stellar photospheres because of a lack of suitable optical lines. On the basis of the fact that Procyon's composition in the other elements is the same as that of the sun and in view of the lack of any recognized Ne abundance anomaly effect in stellar atmospheres (in the manner of the abundances anomalies observed in, for example, Li), we assume with reasonable confidence that Procyon will have a solar abundance of this element.

Procyon was selected for observation by EUVE as a cornerstone wavelength calibration source and as a guest observer (GO) target. Its proximity (3.48 pc) and relatively energetic corona (approximately equal to the sun in its active state, x-ray luminosity $L_x = 10^{28}$ erg/s) make it the brightest effectively nonbinary EUV coronal source available for study; the 11th magnitude companion is too distant to produce any significant interaction effects and as a DF white dwarf would not be the source of any significant EUV or x-ray flux, as confirmed by high-resolution Einstein observations (*15*).

As one of the first observations of late-type stars during the GO phase of the mission, a continuous pointing began on 11 January 1993 UT (universal time) 22:19 and ended on 15 January 1993 UT 00:28; the nominal exposure time was about 100,000 s. The reduction of the raw data into the final flux-calibrated SW, MW, and LW spectra followed standard procedures and is detailed elsewhere (*16*).

The flux, F_{ji}, emitted through a spectral line $j \rightarrow i$ by an optically thin stellar corona can be closely approximated by the integral over the temperature interval, ΔT_{ji}, over which the line flux is nonnegligible (usually, $\log \Delta T_{ji} \sim 0.3$) (in ergs per square centimeter per second):

$$F_{ji} = AK_{ji} \int_{\Delta T_{ji}} G_{ji}(T)\, \overline{n_e^2}\,(T)\, \frac{dV(T)}{dT}\, dT \tag{1}$$

where A is the abundance of the element in question, K_{ji} is a known constant that includes the frequency of the transition and the stellar distance, $n_e(T)$ is the number density of electrons at characteristic temperature T within the volume of the emitting plasma $V(T)$, and $G_{ji}(T)$ is the "contribution" function of the line. This last parameter defines the temperature interval, ΔT_{ji}, over which the line is formed and is dependent on the atomic physics of the particular transition. For most transitions of interest, $G_{ji}(T)$ can be theoretically estimated with fair reliability.

Extracting an elemental abundance from an observed F_{ji} cannot generally be accomplished without detailed knowledge of the

---

J. J. Drake and S. Bowyer, Center for Extreme Ultraviolet Astrophysics, University of California, 2150 Kittredge Street, Berkeley, CA 94720, USA.
J. M. Laming, Sachs Freeman Associates, Landover, MD 20785, USA, and E. O. Hulburt Center for Space Research, Naval Research Laboratory, Code 7674L, Washington, DC 20375, USA.
K. G. Widing, E. O. Hulburt Center for Space Research, Naval Research Laboratory, Code 7674W, Washington, DC 20375, USA.
J. H. M. M. Schmitt, Max-Planck-Institut für Extraterrestrische Physik, 85740 Garching, Germany.
B. Haisch, Lockheed Solar and Astrophysics Laboratory, Department 91-30, Building 252, 3251 Hanover Street, Palo Alto, CA 94304, USA, and Center for Extreme Ultraviolet Astrophysics, University of California, 2150 Kittredge Street, Berkeley, CA 94720, USA.

*To whom correspondence should be addressed.

integrand $n_e^2(T)[dV(T)/dT]$. This quantity is known, historically, as the "differential emission measure." However, if two lines due to different elements can be found whose contribution functions, $G_{ji}(T)$, have the same temperature dependence, then in the expression for the ratio of the line fluxes all terms will cancel except for the elemental abundances and the relevant atomic physics parameters. The ratio of their abundances is obtained directly from the ratio of observed line fluxes. Furthermore, if the two lines are near the same wavelength, then any uncertainties that might arise from the spectrometer calibration and the absorption of radiation in the interstellar medium are removed.

A thorough search of our Procyon spectra revealed the best set of closely spaced features due to low- and high-FIP species with similar temperature dependence to be the closely spaced group of lines Fe XV 243.78 Å, Fe XIII 246.21 Å, and S XI 246.90, 247.13 Å. The S XI line is formed at log $T = 6.25$ and is bracketed by Fe XIII (log $T = 6.2$) and Fe XV (log $T = 6.3$); the Fe/S abundance ratio then lies between the ratios yielded by the Fe XIII and Fe XV lines. Also useful are the regions between 280 and 290 Å, which contain the Fe XV 284.15 Å, S XI 281.42, 285.60, 285.83 Å, and S XII 288.41 Å transitions, and the Si X and S X multiplets near 260 Å. Two other promising candidates whose utility has been pointed out (*8, 17*) are the Mg VI and Ne VI multiplets at ~400 Å and the Ca IX and Ne VII lines near 465 Å. Unfortunately, in our Procyon spectra the 400 Å feature is dominated by stronger Fe XII and Fe XIII lines near 200 Å appearing in second order, rendering it unreliable; we have not pursued this feature further. The moderate resolution and signal-to-noise ratio of the Procyon LW spectrum also renders the Ne VII and Ca IX blend near 465 Å somewhat less useful: The blend is dominated by Ne, making the Ca contribution very difficult to measure. However, a nearby Mg VII line at 434.92 Å provides a reliable comparison for the Ne VII feature.

We measured the individual line intensities by fitting them with Gaussian profiles. All of the above features are partially blended, but because the corona of Procyon is likely to be optically thin, Gaussian fitting allows us to deconvolve readily the relative intensities of the blended lines. We verified that the instrument response of the spectrograph is very close to Gaussian by careful examination of strong, unblended lines such as He II 303.79 Å and Fe XV 284.17 Å. Our analytical fits to the Fe and S lines near 245 Å and between 280 and 290 Å and the Ne-Ca blend at 465 Å, together with residuals, are illustrated in Figs. 1, 2, and 3. The individual line intensity ratios

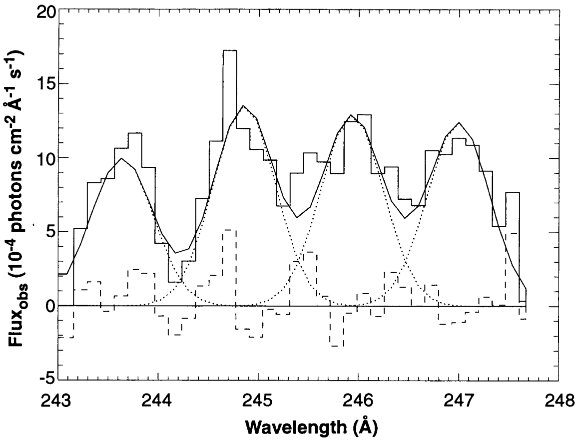

Fig. 1. Observations (solid histogram), fit (solid line), and residuals (dashed histogram) for the Fe XV 243.78 Å, Fe IX 244.91 Å, Fe XIII 246.21 Å, and S XI 246.90, 247.13 Å lines. The individual line components are indicated by the dotted lines. The small wavelength offsets for the Fe XV and Fe XIII lines are caused by known imperfections in the instrument calibration and small detector distortions. Several other strong lines from these ions are visible in the EUVE spectra, making these particular identifications unambiguous. S XI bracketed by Fe XIII and Fe XV (see text). We neglect the likely very small contribution of the Si VI 246.00 Å line to the intensity of Fe XIII 246.21 Å. We based the Gaussian fits and line intensity errors on a χ^2 minimization, using a Levenberg-Marquardt algorithm with single-value decomposition. The errors are estimated from the shape of the χ^2 minimum coming from the singular-value decomposition in the fitting program; this gives essentially the statistical error for clean unblended lines. The fit residuals and intensity errors are consistent with the noise level, which originates from photon noise and background counts. The measured line intensities are listed in Table 1. The Fe/S abundance ratio, based on the average between Fe XV and Fe XIII, and S XI and on the treatment of the atomic physics in (*19*) is Fe/S = 2.4 ± 1.2. This ratio is consistent with the solar photospheric abundance ratio of 2.1 but not with the solar coronal value of 6.8.

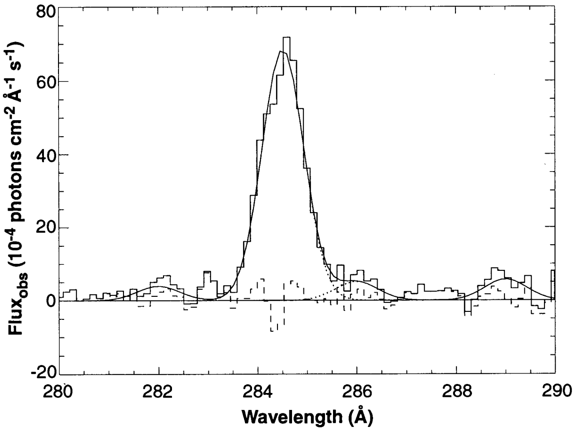

Fig. 2. Observations (solid histogram), fit (solid line), and residuals (dashed histogram) for the Fe XV 284.15 Å, S XI 281.42, 285.60/285.83 Å, and S XII 288.41 Å lines. Fits and intensity errors are as described for Fig. 1, except that the error associated with the S XII 288.42 intensity has been expanded to account for the possible blend with Fe XIV 289.16 Å. A constant wavelength offset of ~0.5 Å is caused by known errors in the spectrometer wavelength calibration. The individual line components in the 284 to 287 Å blend are indicated by the dotted lines. Several other strong lines from these ions are visible in the EUVE spectra, and these identifications are unambiguous: S XII is formed at log $T = 6.3$, like Fe XV, and so a direct comparison between these two is largely independent of the shape of the differential emission measure curve. Abundance ratios are based on the treatment of atomic physics in (*19*).

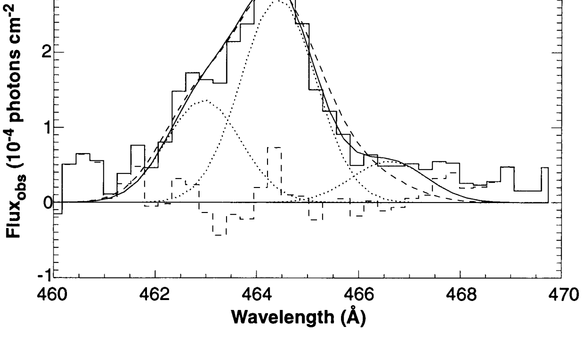

Fig. 3. Observations (solid histogram), fit (solid line), and residuals (dashed histogram) for the Ne VII 465.22 Å, Ca IX 466.23 Å, and unidentified lines at 463.75 and 467.40 Å [the only ones of the unidentified lines appearing in the Skylab atlas (*27*) we find to be statistically significant]. The peaks are displaced from the positions corresponding to the wavelength calibration by a constant offset of −0.8 Å. The dashed curve illustrates the profile resulting from a Ca abundance appropriate to the solar corona. Although this latter curve does not fit the observed data as well as that corresponding to a photospheric Ca abundance, the difference between the two cases is of low significance. We use only the Ne VII line for our abundance analysis.

measured from the fits to the S and Fe lines are also listed in Table 1, together with the derived abundance ratios, for an assumed electron density of 10^{10} cm^{-3}. The S XI lines are slightly sensitive to electron density in this region, in that lower electron densities would give higher emission measures for this ion, and hence a slightly higher Fe/S abundance ratio. The electron density in Procyon's corona has very recently been estimated as $n_e = (5.5 \pm 1.5) \times 10^9$ cm^{-3} (*18*) on the basis of a set of Fe XIV lines; however, if this electron density were used, our results would not be significantly affected.

The abundance ratios determined in this way are consistent with Procyon's photospheric abundances (which are equivalent to the solar photospheric abundances) rather than with solar coronal abundances. From the intensities of the S and Fe lines, using the treatment of the atomic physics in (*19*), we obtain an abundance ratio based on the average between Fe XV and Fe XIII, and S XI of Fe/S = 2.4 ± 1.2. The solar photospheric abundance ratio is 2.0, whereas the coronal value is 6.8 (*8*). Intensities for this same group of lines have also been measured recently from the spectrum of a solar-active region obtained with the Solar EUV Rocket Telescope and Spectrograph (*20*), and also in a full-disk, quiet-sun spectrum (*21*). The abundance ratios obtained in the same way from these spectra are 8 ± 4 and ~5, respectively [no measurement errors are given in (*21*)], essentially the same as the average solar coronal value (*8*). Thus, on the basis of these Fe and S lines, we have a clear indication that the FIP effect in the corona of Procyon is substantially smaller than that in the sun. This result is supported by the Si X 258.39/S X 264.24 ratio and the various intensities ratios available in the region from 280 to 290 Å, as reported in Table 1. These same ratios observed in solar EUV spectra (*20*, *21*) are significantly higher, indicating coronal abundances. These ratios do not include systematic errors arising from the atomic physics, because these cancel in the differential comparison with the sun.

We obtain a similar result from the Ne VII, Ca IX, and Mg VII lines. Because the Ca contribution to the Ne VII and Ca IX blend near 465 Å is rather weak, an accurate Ca/Ne abundance ratio cannot be extracted from this feature. The best fit we obtained for the observed feature, illustrated in Fig. 3, finds essentially no Ca in the blend. The profile corresponding to a coronal Ca abundance ratio is illustrated by the dashed curve. This result is not statistically significant, and instead, we rely on a comparison between Ne VII and a nearby line of Mg VII at 434.92 Å. Because these lines have a small wavelength separation, the relative strengths of the Ne VII and Mg VII lines are weakly dependent on the absorption of EUV flux by neutral hydrogen in the interstellar medium. We accounted for this by using the hydrogen column density from (*22*). The uncertainty in this measurement leads to a further small uncertainty in the Ne VII and Mg VII line intensity ratio of about 10%. The Mg VII 434.92 Å transition is blended with Ne VI 433.18 and 435.65 Å; we have accounted for this by using an emission measure estimated for Ne VI (the mean of those derived for the lines Ne V 416.20 Å and Ne VII 465.22 Å), inasmuch as all other strong lines from this ion (the mutiplets near 400 and 560 Å) are contaminated with higher order features.

The contribution due to the Ne lines amounts to approximately 50% of the total feature flux. The resulting Ne VII and Mg VII line flux ratio and corresponding abundance ratio are listed in Table 1; the uncertainty in the Mg VII line flux due to the subtraction of the Ne VI blend is included in the final result. We obtain an abundance ratio for Mg/Ne of 0.35 ± 0.35. This value is in concordance with Procyon's (and the solar) photospheric ratio rather than with the solar coronal value.

Why would the FIP effect occur in the sun's corona but not in Procyon's? Because the ionization potential separating the low and high FIP is indicative of chromospheric temperatures (~10,000 K), perhaps the answer lies in Procyon's chromosphere. Procyon's chromospheric emission is at, or very near, the "basal" level: The basal-flux stars are the slowest rotators, whose central dynamos are probably not significantly active. However, these stars still exhibit chromospheric emission at levels well above the detection thresholds of instruments such as the International Ultraviolet Explorer (*23*). In the solar chromosphere, the surface flux in regions away from the chromospheric network and plages is close to the basal limit.

It has often been suggested that the basal chromospheric activity level could be due to acoustic heating, in which convective energy is dissipated into the thermal energy of the chromosphere (*23*). According to this scenario, magnetic heating of the basal stars would not be significant. One requirement of potential FIP fractionation models is that the fractionation must occur in relatively short time scales (seconds to minutes) and consequently over small spatial scales (one to tens of kilometers). Otherwise, neutral species would have sufficient time to become ionized during the separation process (*24*). Such small spatial scales can occur quite naturally with magnetic fields but not with acoustic waves. If, then, Procyon's chromosphere is heated predominantly by acoustic means—significantly more so than that of the sun—its corona might not be expected to show any FIP effect. In contrast, the coronal regions of the sun, fed with low-FIP enhanced material from the magnetically active regions in the solar chromosphere, would be expected to show an FIP effect.

The coronal FIP effect is also potentially of central importance to the origin of cosmic rays. It was noticed that the FIP effect observed in the solar corona and wind is very similar to that observed in cosmic rays of medium to low energy (≲100 GeV) (*7*). Suggestions followed that galactic cosmic rays could originate from late-type stellar coronal loss of mass (*6*). These seed particles, enhanced in low-FIP species, are then accelerated to relativistic energies by diffusive shock acceleration (*25*) provided by, for example, supernova remnants in interstellar space.

Table 1. Summary of lines used in the analysis, their observed intensity ratios in Procyon, and corresponding abundance ratios.

Abundance diagnostic	log *T*	Intensity ratio	Abundance ratio (by number)		
			Solar photosphere*	Solar corona†	Procyon corona
Fe XV 284.15 Å : S XII 288.41 Å	6.3	12 ± 6	Fe/S = 2.0	6.8	1.9 ± 1.0
Fe XIII 246.21 Å : S XI 246.90, 247.13 Å	6.2–6.25	1.2 ± 0.6	Fe/S = 2.0	6.8	1.7 ± 0.9
Fe XV 243.78 Å : S XI 246.90, 247.13 Å	6.25–6.3	0.96 ± 0.5	Fe/S = 2.0	6.8	3.1 ± 1.5
Fe XV 284.15 Å : S XI 281.42 Å	6.25–6.3	17 ± 6	Fe/S = 2.0	6.8	0.95 ± 0.3
Fe XV 284.15 Å : S XI 285.60, 285.83 Å	6.25–6.3	13 ± 5	Fe/S = 2.0	6.8	2.7 ± 1.0
Si X 258.39 Å : S X 264.24 Å	6.1–6.15	0.94 ± 0.5	Si/S = 2.1	6.8	1.4 ± 0.7
Mg VII 434.92 Å : Ne VII 465.22 Å	5.7	0.077 ± 0.07	Mg/Ne = 0.31	1.2	0.35 ± 0.35

*From (*28*). †From (*8*).

It has been pointed out (*26*) that this scenario is particularly appealing, because other nonstellar injection models suffer the disadvantage of both having to account for the fractionation through other means and facing the prospect that the remarkable similarity between the cosmic-ray source composition and the composition of solar energetic particles is purely accidental. However, this hypothesis is based entirely on extrapolation of the solar case, because before now it has not been possible to determine the abundances of elements in the coronae of other stars. Our failure to detect a similar FIP effect in the corona of Procyon provides evidence that the FIP effect is not a ubiquitous signature of late-type stellar coronae.

REFERENCES AND NOTES

1. S. R. Pottasch, *Astrophys J.* **137**, 945 (1963).
2. A. Mogro-Campero and J. A. Simpson, *ibid.* **171**, L5 (1972).
3. A. B. C. Walker, H. R. Rugge, K. Weiss, *ibid.* **194**, 471 (1974).
4. H. R. Rugge and A. B. C. Walker, *ibid.* **203**, L139 (1976).
5. J. H. Parkinson, *Astron. Astrophys.* **57**, 185 (1977).
6. J.-P. Meyer, *Astrophys. J. Suppl. Ser.* **57**, 172 (1985).
7. M. Cassé and P. Goret, *Astrophys. J.* **221**, 703 (1978).
8. U. Feldman, *Phys. Scr.* **46**, 202 (1992).
9. S. Bowyer and R. F. Malina, in *Extreme Ultraviolet Astronomy*, R. F. Malina and S. Bowyer, Eds. (Pergamon, New York, 1991), p. 94.
10. R. Griffin, *Mon. Not. R. Astron. Soc.* **155**, 139 (1971).
11. J. Tomkin and D. L. Lambert, *Astrophys. J.* **223**, 937 (1978).
12. K. Kato and K. Sadakane, *Astron. Astrophys.* **167**, 111 (1986).
13. M. Steffen, *Astron. Astrophys. Suppl. Ser.* **59**, 403 (1985).
14. B. Edvardsson *et al.*, *Astron. Astrophys.* **275**, 101 (1993).
15. J. H. M. M. Schmitt *et al.*, *Astrophys. J.* **290**, 307 (1985).
16. B. Haisch, J. J. Drake, J. H. M. M. Schmitt, *ibid.* **421**, L39 (1994).
17. K. G. Widing and U. Feldman, *ibid.* **334**, 1046 (1989).
18. J. H. M. M. Schmitt, B. M. Haisch, J. J. Drake, *Science* **265**, 1420 (1994).
19. P. L. Dufton, personal communication; D. R. Flower and H. Nussbaumer, *Astron. Astrophys.* **31**, 353 (1974); B. C. Fawcett and H. E. Mason, *At. Data Nucl. Data Tables* **43**, 245 (1989); H. E. Mason and A. K. Bhatia, *Mon. Not. R. Astron. Soc.* **184**, 423 (1978); D. F. Flower and H. Nussbaumer, *Astron. Astrophys.* **42**, 265 (1975).
20. R. J. Thomas and W. M. Neupert, *Astrophys. J. Suppl. Ser.* **91**, 461 (1994).
21. M. Malinovsky and L. Heroux, *Astrophys. J.* **181**, 1009 (1973).
22. J. Murthy *et al.*, *ibid.* **315**, 675 (1987).
23. C. J. Schrijver, *Astron. Astrophys.* **180**, 241 (1987).
24. R. von Steiger and J. Geiss, *ibid.* **225**, 222 (1989).
25. W. I. Axford, E. Leer, K. G. Skandron, *Proc. 15th Int. Cosmic Ray Conf.* **11**, 32 (1977).
26. H. Bloemen, in *Interstellar Processes*, D. J. Hollenbach and H. A. Thronson Jr., Eds. (Reidel, Dordrecht, Netherlands, 1987), p. 143.
27. U. Feldman, J. D. Purcell, B. C. Dohne, *NRL Rep. 90-4100* and *NRL Rep. 91-4100* (Naval Research Laboratory, Washington, DC, 1987).
28. E. Anders and N. Grevesse, *Geochim. Cosmochim. Acta* **53**, 197 (1989).
29. We thank G. Doschek, U. Feldman, K. Strong, and J. Saba for useful discussions and the EUVE Science Team for advice and support. We thank the referees for pertinent comments, which improved the manuscript. J.J.D. was supported by National Aeronautics and Space Administration grant AST91-15090 administered by the Center for Extreme Ultraviolet Astrophysics, University of California.

18 August 1994; accepted 28 December 1994

Conducting Layered Organic-Inorganic Halides Containing ⟨110⟩-Oriented Perovskite Sheets

D. B. Mitzi,* S. Wang, C. A. Feild, C. A. Chess, A. M. Guloy

Single crystals of the layered organic-inorganic perovskites, $[NH_2C(I){=}NH_2]_2(CH_3NH_3)_m Sn_m I_{3m+2}$, were prepared by an aqueous solution growth technique. In contrast to the recently discovered family, $(C_4H_9NH_3)_2(CH_3NH_3)_{n-1}Sn_nI_{3n+1}$, which consists of ⟨100⟩-terminated perovskite layers, structure determination reveals an unusual structural class with sets of *m* ⟨110⟩-oriented $CH_3NH_3SnI_3$ perovskite sheets separated by iodoformamidinium cations. Whereas the $m = 2$ compound is semiconducting with a band gap of 0.33 ± 0.05 electron volt, increasing *m* leads to more metallic character. The ability to control perovskite sheet orientation through the choice of organic cation demonstrates the flexibility provided by organic-inorganic perovskites and adds an important handle for tailoring and understanding lower dimensional transport in layered perovskites.

Recent interest in organic-inorganic multilayer perovskites stems from the flexibility to use organic layers to tailor magnetic (*1*, *2*), optical (*3*, *4*), thermochromic (*5*), or structural (*6*) properties of adjacent nonconducting metal halide perovskite sheets. Typically, these self-assembling structures consist of single ⟨100⟩-terminated perovskite sheets alternating with alkylammonium bilayers, with the alkyl chains extending into the space between layers and van der Waals interactions between chains holding the layers together. More complicated organic cations have also been incorporated, including those with benzene rings and unsaturated hydrocarbon tails (*4*, *7*). The ability to polymerize the organic layer (*7*, *8*) or to study conformational changes within long-chain alkylammonium bilayers (*9*) provides further flexibility and interest.

Recently, a family of conducting layered organic-inorganic perovskites, $(C_4H_9NH_3)_2(CH_3NH_3)_{n-1}Sn_nI_{3n+1}$ ($n = 1$ to 5), was found (*10*) in which *n* ⟨100⟩-terminated $CH_3NH_3SnI_3$ perovskite sheets alternate with butylammonium bilayers. These conducting non–oxide-layered perovskites share many of the structural features of the cuprate superconductors and other conducting layered-oxide perovskites (which also consist of ⟨100⟩ perovskite sheets). In addition, these systems are natural (self-assembling) analogs to semiconductor quantum-well multilayers, with the perovskite layers acting as wells and the longer-chain alkyl layers forming barrier layers. Observation of enhanced exciton binding energies in both the lead(II) and tin(II) analogs of these layered perovskites highlight the two-dimensional nature and the effect of dielectric modulation (*3*, *11*).

In this report, we discuss the synthesis, structure, and transport properties of a class of conducting layered halides, $[NH_2C(I){=}NH_2]_2(CH_3NH_3)_mSn_mI_{3m+2}$ ($m = 2$ to 4), that consists of *m* $CH_3NH_3SnI_3$ perovskite layers terminating on a ⟨110⟩ crystallographic plane, rather than on the usual ⟨100⟩ plane. This structure appears to be stabilized by the interposed layers of iodoformamidinium cations, which orient along the channels provided by the ⟨110⟩ perovskite surfaces. The ability to form either ⟨100⟩- or ⟨110⟩-terminated perovskite sheets through the choice of organic cation in the initial crystal growth solution (in this case, butylammonium versus iodoformamidinium) demonstrates an additional degree of flexibility within the family of organic-inorganic perovskites. Many of the related ⟨100⟩-terminated conducting layered perovskites—including the oxides $(La_{1-x}Sr_x)_{n+1}Mn_nO_{3n+1}$ (*12*), $La_{n+1}Ni_nO_{3n+1}$ (*13*), and $Ba_{n+1}Pb_nO_{3n+1}$ (*14*) as well as the halide $(C_4H_9NH_3)_2(CH_3NH_3)_{n-1}Sn_nI_{3n+1}$ (*10*)—undergo a semiconductor-metal transition with increasing *n*. We find a similar trend in the ⟨110⟩-terminated layered perovskites.

Crystals of each tin(II)-based layered perovskite were grown in an argon atmosphere by slow cooling from concentrated aqueous hydriodic acid solutions of $CH_3NH_2{\cdot}HI$, NH_2CN, and SnI_2 (*15*). The chemistry of cyanamide in this synthesis is in itself unusual. Although anhydrous reaction between nitriles (RCN) and hydrogen halides (HX) generally results in the nucleophilic attack of X^- on the nitrile triple bond (resulting in an

---

D. B. Mitzi, C. A. Feild, C. A. Chess, IBM T. J. Watson Research Center, Post Office Box 218, Yorktown Heights, NY 10598, USA.
S. Wang and A. M. Guloy, Department of Chemistry and Texas Center for Superconductivity, University of Houston, Houston, TX 77204-5641, USA.

*To whom correspondence should be addressed.